










Automated Ventricular System Segmentation in CT Images of Deformed Brains Due to Ischemic and Subarachnoid Hemorrhagic Stroke

E. Ferdian^{1,2,3} , A.M. Boers^{1,2,4} , L.F. Beenen² ,
B.M. Cornelissen^{1,2,4} , I.G. Jansen² , K.M. Treurniet² ,
J. Borst² , C.B. Majoie² , and H.A. Marquering^{1,2} 

- ¹ Department of Biomedical Engineering and Physics, Academic Medical Center, Meibergdreef 15, Amsterdam, The Netherlands
edwardferdian03@gmail.com
- ² Department of Radiology, Academic Medical Center, Meibergdreef 15, Amsterdam, The Netherlands
- ³ Department of Medical Informatics, Academic Medical Center, Meibergdreef 15, Amsterdam, The Netherlands
- ⁴ Department of Robotics and Mechatronics, University of Twente, Hallenweg 15, Enschede, The Netherlands

Abstract. Accurate ventricle segmentation is important for reliable automated infarct localization, detection of early ischemic changes, and localization of hemorrhages. The purpose of this study was to develop a robust and accurate ventricle segmentation method in image data of ischemic and hemorrhagic stroke patients. Early follow-up non-contrast CT image data of 35 patients with a clinical diagnosis of ischemic stroke or subarachnoid hemorrhage were collected. We proposed a ventricle segmentation method based on a combination of active contours and an atlas-based segmentation. Ground truth was obtained by manual delineation of the ventricles by 4 observers with corrections by 2 experienced radiologists. Accuracy of the automated method was evaluated by calculation of the intraclass correlation coefficients, Dice coefficients, and by Bland-Altman analysis. The intraclass correlation coefficient for the automated method compared with the reference standard was excellent (0.93). The Dice coefficients was 0.79 [IQR: 0.72–0.84]. Bland-Altman analysis showed a mean difference of 2 mL between the automatic and manual measurements, with broad limits of agreement ranging from –18 to 15 mL. The automated ventricle segmentation showed an excellent correlation and high accuracy compared to the manual reference measurement. This approach is suitable for reliable ventricle segmentation even in stroke patients with a severely deformed brain.

Keywords: Ventricular system · Segmentation · Deformed brain · CT · Stroke · Subarachnoid hemorrhage

1 Introduction

Stroke is the leading cause of disability and second leading cause of death worldwide [1]. Diagnosis and treatment decisions of patients with ischemic and hemorrhagic stroke depend heavily on radiological imaging. Recently, various automated methods of CT image analysis of stroke patients have been introduced: infarct core quantification [2], hemorrhage quantification [3], and ASPECTS scoring [4]. In these methods, accurate ventricle segmentation plays a key role in correctly locating and quantifying these lesions.

Several methods have been proposed for segmenting the ventricles either in healthy or slightly deformed brains. These methods were based on techniques such as region growing [5, 6], cognition network [7], low-level segmentation combined with high-level template matching [8], and active model-based segmentation [9–11]. In stroke patients, severe deformation of the brain is quite common. However, this deformation issue is not normally addressed in existing literatures. In general, ventricle segmentation for stroke patients shared a common trait, such as difficulty in distinguishing infarct regions from the ventricles due to similar intensity and also the stroke regions are often located adjacent to the ventricle. For example, in ischemic stroke patients, the density of infarct regions can be in the proximity of that of cerebrospinal fluid (CSF) within the ventricles. Moreover, in other cases such as hemorrhagic stroke, blood often leaks inside the ventricles, yielding problems with existing segmentation methods.

Up to now, only several ventricle segmentation methods that are dedicated for stroke patients have been proposed [10, 12, 13]. These studies, however, focused on either ischemic or hemorrhagic stroke patients, but not both. We tried to take an approach from the perspective of brain deformation due to stroke.

The aim of our study was to design a robust automated ventricular segmentation method for CT images suitable for patients with severe brain deformation due to ischemic or subarachnoid hemorrhagic stroke to aid subsequent image analyses, such as infarct quantification and subarachnoid hemorrhage detection tools.

2 Materials and Methods

2.1 Patient Selection

Early follow-up whole-brain non-contrast CT (NCCT) image data of 50 patients with a clinical diagnosis of ischemic stroke or subarachnoid hemorrhage (SAH) were collected. Brain image data with 5 mm slice thickness were used, resulting in volumes with 24–51 slices. We retrieved 1-week follow-up NCCT image data of ischemic stroke patients from the MR CLEAN database [14], while baseline NCCT image data of SAH patients were retrieved from the local data base from our institute. From our initial image database of 50 patients, patients with hemicraniectomy ($n = 4$) and incomplete image data ($n = 11$) were excluded. The image data were anonymized before analyses.

2.2 Method Overview

The proposed ventricle segmentation approach is based on localized region-based active contours [15]. Since active contours require a good initial estimation, we divided our method into two stages: (1) initial contour estimation using atlas-based ventricle segmentation and (2) active contours based ventricle segmentation.

First stage: Initial contour estimation. In the first stage, we performed an atlas-based segmentation on skull-stripped brain images. The skull-stripping algorithm is performed using a thresholding operation [3] to exclude the skull and non-brain tissues from the subject image. We considered regions >100 HU as the skull and excluded them from the brain image. Registrations were performed using open source software Elastix (version 4.3; <http://elastix.isi.uu.nl>) [16, 17] with mutual information set as similarity measure. Rigid, affine, and B-splined (grid spacing: 15 mm) transformations were applied sequentially. Subsequently, we applied the transformation parameter from the registered image to the ventricle atlas. For this purpose, we used an in-house-developed ventricle atlas that contains labels of the two lateral ventricles, third ventricle, fourth ventricle, and nonventricular CSF regions. The atlas-based segmentation resulted in masks of the ventricles of the patient image (See Fig. 1).

Subsequently in the masked areas, CSF and hemorrhage within the ventricles were segmented using density-based thresholding. All voxels within the masked image with a density of 0–16HU and 55–90HU were labeled as CSF and intraventricular blood respectively. Voxels with a density between 16 and 55 HU were considered as normal brain tissue.

The result of the procedure described above included false positives, which consist of adjacent infarct regions, adjacent hemorrhagic regions, and non-ventricular CSF regions, which mostly occur around the segmentation of lateral ventricles. To detect false positive regions, in every axial slice of the lateral ventricles, a connected component analysis was performed, subsequently followed by region growing operation on each of the components. The region growing was performed to include neighboring pixels with density slightly range slightly higher than the CSF segmentation [0–19 HU] to ensure connectivity to nonventricular CSF regions. When the result of region growing overlaps more than 75% with the original segmentation, the seed component is considered as a true positive. On the other hand, when the result spread towards previously unsegmented region, the component is removed from the original segmentation (See Fig. 2).

Second Stage: Active contours based ventricle segmentation. Localized region-based active contours was used in the refinement stage [15, 18]. Uniform energy modeling was used as internal energy measure. The foreground (CSF/ventricle) and background (white matter, gray matter) are modeled as constant intensity values represented by their means. Because of the large differences between in-plane resolution and slice thickness, active contours was applied in 2D axial slices rather than in a 3D volume, with the following parameters: radius of local area ($\text{rad} = 10$), coefficient curvature regularization term ($\alpha = 0.001$), smoothness ($\epsilon = 10$), number of iterations ($n = 500$). This 2D approach also allowed the active contours to filter out small noise regions.

We first performed active contours on the main slice of the lateral ventricles. We defined the main slice as the axial slice that contains the largest two-dimensional (2D) connected component from the initial estimation. For the main slice, the initial segmentation from the previous stage is used as the initial contour. The segmentation result from the main slice is then used to calculate patient-specific CSF threshold. This segmentation result is propagated to its adjacent inferior and superior slices to be used as an input for the next initial contour.

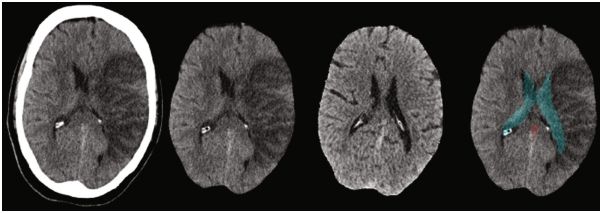


Fig. 1. Examples of atlas-based segmentation on a skull-stripped image (First column shows the original brain image with skull, second column shows the brain image without skull (regions >100 HU excluded), third column shows the registered image, fourth column shows atlas-based segmentation on the skull-stripped image).

Subsequently, the third, fourth, and the remainder of lateral ventricles slices were segmented using active contours in a propagative manner. This order was chosen due to the interconnectedness of the ventricle regions. To compensate to the large distance between slices, initial contours were obtained by combining the estimation from the first stage and the projection from the segmentation from the previous slice, masked with the patient-specific CSF threshold.

Finally, intraventricular calcification regions were identified to be included as ventricles in the segmentation. In slices that contain the posterior and inferior horns (axial slices between the roof of the 3rd and roof of the 4th ventricle); dilation morphological operation with a structuring element of 5×5 mm was applied to include calcifications.

2.3 Accuracy

Ventricles in 35 CT images (17 ischemic stroke and 18 SAH patient images) were manually delineated by trained observers and when necessary corrected by experienced radiologists (L.F.B and C.B.M, both with >10 years of experience). The manually delineated ventricles were used as reference standard to evaluate the accuracy of our method.

The accuracy was measured by calculating the Intraclass Correlation Coefficient (ICC) and performing Bland-Altman analysis. Furthermore, the Dice similarity coefficient (DSC) between the automated and manual segmentation was determined to calculate the overlap.

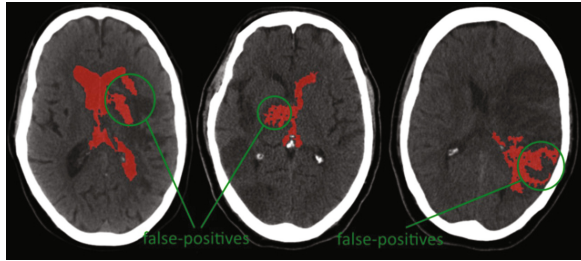


Fig. 2. Illustration of false-positives regions that were detected by region-growing algorithm. The component which was used as the seed is labelled as a potential leak and excluded from the refinement process

3 Results

The automated segmentation was successfully performed on all 35 NCCT images (17 ischemic stroke and 18 SAH patients) without any manual intervention or adjustment. The median ventricle volume was 33.2 mL [IQR: 23.7–43.2] and 28.1 mL [IQR: 25.5–45.9], according to the automated and manual delineations, respectively. The ventricle segmentation took 10–20 min per patient to complete on a Core i7, 2.67 GHz PC with 6 GB RAM. This execution time is without the time to perform the atlas-based

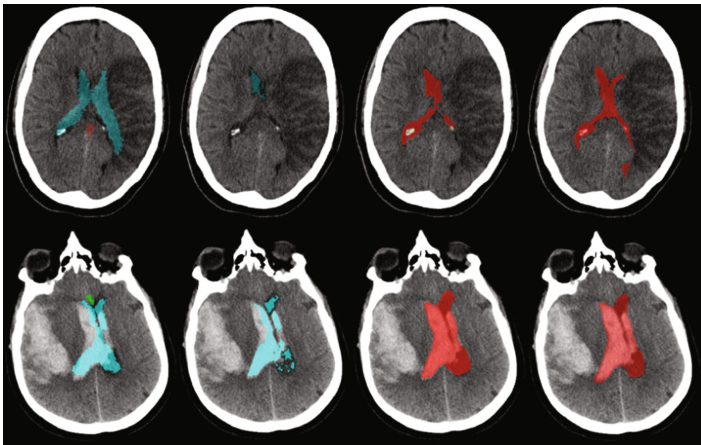


Fig. 3. Examples of segmented ventricles (1st column represents the original atlas-based segmentations with false-positive regions. The 2nd column represents the segmentations after removal of the false-positive regions. The 3rd column represents the delineations by experts, which was used as a reference standard). On the first and second column cyan represents the lateral ventricles, green and red represent non-ventricular CSF regions. On the third and fourth column red represents the final segmentation. The first and second row show ischemic and subarachnoid hemorrhagic stroke patient images, respectively. (Color figure online)

segmentation, which took 15–30 min per patient. Some segmentation results are shown in Fig. 3.

The ICC of the automatic and manual ventricle volume measurement was excellent: 0.93 (95%CI 0.88–0.96; $p < 0.001$). Bland-Altman analysis indicated a mean difference in ventricle volume of 2 mL between the automatic and manual measurements, with limits of agreement ranging from –18 to 15 mL. The Dice coefficient of the manual and automatic measurements had a median of 0.79 [IQR: 0.72–0.84]. Overall, the accuracy for segmentations in ischemic stroke is higher compared to the SAH patients (ICC: 0.97 vs 0.88, DSC: 0.82 vs 0.72). Bland-Altman analysis also show narrower limits of agreement in the ischemic stroke segmentation compared to the SAH (–10 to 9.6 mL as opposed to –24 to 17 mL). See Table 1.

Our method successfully distinguished between CSF and infarcts or hemorrhages. However, some minor leakages were still observed in 5 (14.3%) of the segmentations, for example into non-ventricular CSF regions, infarcts, and hemorrhages. Additionally, in some cases the proposed method did not recognize narrow or small regions such as the cerebral aqueduct between the third and fourth ventricle.

4 Discussion

We introduced an automated ventricle segmentation method in NCCT images of patients with ischemic stroke or SAH with a severely deformed brain. The segmentation method is fully automated and applicable to severely deformed brain. Evaluation with 35 patients showed a good agreement with manual assessment, with limits of agreement between –18 and 15 mL compared with the manual reference method. The accuracy of the automated method was high.

To our knowledge, the presented method is the first that is robust in segmenting ventricles in severely deformed brains for both ischemic stroke and SAH patients. Compared to previous methods [10, 12, 13], the accuracy of our method for ischemic stroke patients is slightly lower. However, it should be noted that we only selected severely deformed ventricles in our study. In addition, the presented method works well in a wide range of ventricle size from our sample data. Previous studies reported some difficulties in segmenting small sized ventricles [12], while in other studies smaller size ventricles, such as the fourth ventricle [7, 9, 11] and third ventricle [5] were excluded in the process.

Table 1. Accuracy of manual ventricle volume measurement and comparison of the manual and automated segmentation.

Segmentation	Intraclass correlation (95% CI)	Dice coefficient (median and IQR)	Bland-Altman limits of agreement (mL)	# samples
Automated vs manual	0.93 (0.88–0.96)	0.79 [IQR: 0.72–0.84]	–18–15	35
Automated vs manual (ischemic)	0.97 (0.93–0.99)	0.82 [IQR: 0.78–0.86]	–10–9.6	17
Automated vs manual (SAH)	0.88 (0.76–0.95)	0.72 [IQR: 0.64–0.77]	–24–17	18

Recent study from Qian et al. [13] showed an impressive result in segmenting ventricle and distinguishing stroke regions. However, we find that the method relies on symmetry of the brain which is not often the case for severely deformed brain. Moreover, we tried to generalize our method to cover different cases of stroke and not specific to ischemic stroke.

We used atlas based segmentation for our initial contours by performing non-linear registration on skull-stripped brain images. We found this approach suitable for our cases with deformed brain. Other approaches, such as the above mentioned symmetric based approach is not suitable for our dataset. In terms of active contours segmentation, we used a propagated 2D approach instead of 3D approach in order to detect leaking as early as possible. By putting a size threshold on the contours, the extent of leakage is minimized. The novelty of our method lies in the removal of false-positives using region-growing algorithm. We took advantage of the leaking characteristics of region growing to detect false-positive segmentations.

In our study, we have chosen to develop a method that allows the segmentation of severely deformed ventricles for both ischemic stroke as well as subarachnoid hemorrhage patients. Alternatively, it could also be possible to combine two different segmentation techniques that are optimized for either ischemic stroke or subarachnoid hemorrhages and select the optimal result retrospectively. However, it was beyond the scope of this study to explore this strategy.

There are a few limitations in our method. Our method is computationally demanding. Even though the localized region-based active contours has shorter computation time compared to the global variant [15], our implementation took around 20–30 min per patient. A limitation is that we evaluated the accuracy on the same image data set as was used for its development. This may, therefore, overestimate its accuracy. Because of the limited number of severely deformed ventricles, we used the same dataset for both training and evaluation purposes.

Using our method, the accuracy of the segmentation in SAH patients was somewhat lower compared to ischemic stroke patients. In SAH patients, there is commonly a large amount of blood within or adjacent to the ventricle, especially around the posterior and inferior horns. The ventricle segmentation is the most difficult for these patients because of the indistinct boundary between intra-and-extra ventricular hemorrhages.

This automated approach enables a reproducible and observer-independent analysis. Our method offers the following improvements compared to previously presented methods: complete segmentation of all ventricles (lateral, third, and fourth ventricles), accurate in patients with subarachnoid hemorrhages, and a control to prevent excessive segmentation leakage to infarct and non-ventricular CSF regions.

There is still some room for improvement. Future work may address improvement of the initial contour estimation, reduction of computation time of the active contours, and improvement in the detection of intra vs. extra-ventricular hemorrhages.

We have presented a robust automatic method for ventricle segmentation in CT images of ischemic stroke and SAH patients with severely deformed brains. The segmentation accuracy is sufficient to assist additional automated methods that require ventricle segmentation such as the detection of infarcts and subarachnoid hemorrhages.

References

1. Towfighi, A., Saver, J.L.: Stroke declines from third to fourth leading cause of death in the United States: historical perspective and challenges ahead. *Stroke* **42**, 2351–2355 (2011). doi:[10.1161/STROKEAHA.111.621904](https://doi.org/10.1161/STROKEAHA.111.621904)
2. Boers, A.M., Marquering, H.A., Jochem, J.J., et al.: Automated cerebral infarct volume measurement in follow-up noncontrast CT scans of patients with acute ischemic stroke. *Am. J Neuroradiol.* **34**, 1522–1527 (2013). doi:[10.3174/ajnr.A3463](https://doi.org/10.3174/ajnr.A3463)
3. Boers, A.M., Zijlstra, I.A., Gathier, C.S., et al.: Automatic quantification of subarachnoid hemorrhage on noncontrast CT. *Am. J. Neuroradiol.* **35**, 2279–2286 (2014). doi:[10.3174/ajnr.A4042](https://doi.org/10.3174/ajnr.A4042)
4. Stoel, B.C., Marquering, H.A., Staring, M., et al.: Automated brain CT densitometry of early ischemic changes in acute stroke. *AJNR Am. J. Neuroradiol.* (2013). doi:[10.1117/1.JMI.2.1.014004](https://doi.org/10.1117/1.JMI.2.1.014004)
5. Schnack, H.G., Hulshoff Pol, H.E., Baaré, W.F.C., et al.: Automatic segmentation of the ventricular system from MR images of the human brain. *Neuroimage* **14**, 95–104 (2001). doi:[10.1006/nimg.2001.080](https://doi.org/10.1006/nimg.2001.080)
6. Xia, Y., Hu, Q., Aziz, A., Nowinski, W.L.: A knowledge-driven algorithm for a rapid and automatic extraction of the human cerebral ventricular system from MR neuroimages. *Neuroimage* **21**, 269–282 (2004). doi:[10.1016/j.neuroimage.2003.09.029](https://doi.org/10.1016/j.neuroimage.2003.09.029)
7. Schönmeier, R., Prvulovic, D., Rotarska-Jagiela, A., et al.: Automated segmentation of lateral ventricles from human and primate magnetic resonance images using cognition network technology. *Magn. Reson. Imaging* **24**, 1377–1387 (2006). doi:[10.1016/j.mri.2006.08.013](https://doi.org/10.1016/j.mri.2006.08.013)
8. Chen, W., Smith, R., Ji, S.-Y., et al.: Automated ventricular systems segmentation in brain CT images by combining low-level segmentation and high-level template matching. *BMC Med. Inform. Decis. Mak.* **9**, S4 (2009). doi:[10.1186/1472-6947-9-S1-S4](https://doi.org/10.1186/1472-6947-9-S1-S4)
9. Fan, Y., Jiang, T., Evans, D.J.: Volumetric segmentation of brain images using parallel genetic algorithms. *IEEE Trans. Med. Imaging* **21**, 904–909 (2002). doi:[10.1109/TMI.2002.803126](https://doi.org/10.1109/TMI.2002.803126)
10. Liu, J., Huang, S., Ihar, V., et al.: Automatic model-guided segmentation of the human brain ventricular system from CT images. *Acad. Radiol.* **17**, 718–726 (2010). doi:[10.1016/j.acra.2010.02.013](https://doi.org/10.1016/j.acra.2010.02.013)
11. Etyngier, P., Ségonne, F., Keriven, R.: Active-contour-based image segmentation using machine learning techniques. In: Ayache, N., Ourselin, S., Maeder, A. (eds.) *MICCAI 2007*. LNCS, vol. 4791, pp. 891–899. Springer, Heidelberg (2007). doi:[10.1007/978-3-540-75757-3_108](https://doi.org/10.1007/978-3-540-75757-3_108)
12. Poh, L.E., Gupta, V., Johnson, A., et al.: Automatic segmentation of ventricular cerebrospinal fluid from ischemic stroke CT images. *Neuroinformatics* **10**, 159–172 (2012). doi:[10.1007/s12021-011-9135-9](https://doi.org/10.1007/s12021-011-9135-9)
13. Qian, X., Lin, Y., Zhao, Y., et al.: Objective ventricle segmentation in brain CT with ischemic stroke based on anatomical knowledge. *Biomed. Res. Int.* **2017**, 1–11 (2017). doi:[10.1155/2017/8690892](https://doi.org/10.1155/2017/8690892)
14. Berkhemer, O., Fransen, P., Beumer, D., et al.: A randomized trial of intraarterial treatment for acute ischemic stroke. *New. Engl. J. Med.* **372**, 11–20 (2014). doi:[10.1056/NEJMoa1411587](https://doi.org/10.1056/NEJMoa1411587)
15. Lankton, S., Tannenbaum, A.: Localizing region-based active contours. *IEEE Trans. Image Process.* **17**, 2029–2039 (2008). doi:[10.1109/TIP.2008.2004611](https://doi.org/10.1109/TIP.2008.2004611)
16. Klein, S., Staring, M., Murphy, K., et al.: Elastix: a toolbox for intensity-based medical image registration. *IEEE Trans. Med. Imaging* **29**, 196–205 (2010)

17. Shamonin, D.P., Bron, E.E., Lelieveldt, B.P.F., et al.: Fast parallel image registration on CPU and GPU for diagnostic classification of Alzheimer's disease. *Front. Neuroinform.* **7**, 50 (2013)
18. Pang, J.: Localized Active Contour (2014). <http://uk.mathworks.com/matlabcentral/fileexchange/44906-localized-active-contour>